HHS Public Access

Author manuscript

Nature. Author manuscript; available in PMC 2012 September 22.

Published in final edited form as:

Nature. ; 483(7390): 465–469. doi:10.1038/nature10877.

MEGF10 AND 11 MEDIATE HOMOTYPIC INTERACTIONS REQUIRED FOR MOSAIC SPACING OF RETINAL NEURONS

Jeremy N. Kay, **Monica W. Chu**, and **Joshua R. Sanes**[+]

Center for Brain Science and Department of Molecular and Cellular Biology, Harvard University, 52 Oxford Street, Cambridge MA, 02138

Abstract

In many parts of the nervous system, neuronal somata display orderly spatial arrangements[1]. In the retina, neurons of numerous individual subtypes form regular arrays called mosaics: they are less likely to be near neighbors of the same subtype than would occur by chance, resulting in "exclusion zones" that separate them[1-4]. Mosaic arrangements provide a mechanism to distribute each cell type evenly across the retina, ensuring that all parts of the visual field have access to a full set of processing elements[2]. Remarkably, mosaics are independent of each other: while a neuron of one subtype is unlikely to be adjacent to another of the same subtype, there is no restriction on its spatial relationship to neighboring neurons of other subtypes[5]. This independence has led to the hypothesis that molecular cues expressed by specific subtypes pattern mosaics by mediating homotypic (within-subtype) short-range repulsive interactions[1,4-9]. To date, however, no molecules have been identified that show such activity, so this hypothesis remains untested. Here, we demonstrate that two related transmembrane proteins, MEGF10 and MEGF11, play critical roles in formation of mosaics by two retinal interneuron subtypes, starburst amacrine cells (SACs) and horizontal cells (HCs). MEGF10/11 and their invertebrate relatives *C. elegans* CED-1 and *Drosophila* Draper, have hitherto been studied primarily as receptors necessary for engulfment of debris following apoptosis or axonal injury[10-14]. Our results demonstrate that members of this gene family can also serve as subtype-specific ligands that pattern neuronal arrays.

The retina contains over 70 neuronal subtypes, divided into broad categories of photoreceptors, interneurons and retinal ganglion cells[15] To seek molecules involved in cell-cell recognition events during retinal circuit assembly, we purified thirteen subtypes of retinal neurons from transgenic mice and used microarrays to inventory the genes they expressed[16,17]. We collected cells at postnatal day (P)6, a time at which synapse formation and mosaic refinement are underway. From this dataset we identified genes selectively expressed by specific subtypes, including SACs, an interneuronal subtype that plays critical

---

[+]Correspondence: sanesj@mcb.harvard.edu.

AUTHOR CONTRIBUTIONS

J.N.K. and J.R.S. designed experiments and wrote the paper. J.N.K. and M.W.C. performed experiments. J.N.K. performed data analysis. J.R.S. supervised the project.

The authors declare no competing interests.

roles in motion detection[18]. The ~100 genes that met our criteria for selective SAC expression included most known SAC markers as well as potential new markers (Fig. 1a; Table S1). Thirty-one of the novel genes were tested by in situ hybridization or immunohistochemistry in combination with SAC markers such as choline acetyltransferase (ChAT) or calbindin[19]. This secondary screen yielded 26 genes (Table S1), among which were two homologues, *Megf10* and *Megf11*. These genes encode transmembrane proteins with multiple EGF-like domains, a single membrane-spanning region, and a cytoplasmic domain with several binding sites for signal transduction components[10,13] (Fig. S1). At P5-6, both genes were strongly expressed in SACs (Fig. 1a-c). Both were also expressed in HCs, which were not part of the dataset.

SACs are present in both the inner nuclear and ganglion cell layers, and form independent mosaics in each[5]. These mosaics develop during late embryonic (E) stages, as newborn SACs migrate from the site of their birth, the outer neuroblast layer, to their final laminar locations. SACs begin to exhibit mosaic spacing upon arrival at their destinations, presumably due to contacts with their homotypic neighbors[8,9]. As new SACs are added to the array, local cellular rearrangements maintain mosaic spacing[1,4,9]. Mosaic spacing is maintained even as SAC dendrites grow to overlap with those of their neighbors[20]; thus, mosaicism is distinct from the phenomenon called tiling, which minimizes dendritic overlap[15]. Co-staining at E16 with the early SAC marker Islet1[9,21] demonstrated that newborn SACs activated *Megf10* expression as they finished their migration and became integrated into mosaics (Fig. 1d). *Megf10* expression persisted in SACs from this time through the first postnatal week, and began in HCs at P0 (Fig. S1 and data not shown). In the second postnatal week, *Megf10* was downregulated in neurons but appeared in Müller glia (Fig. 1e), consistent with previous reports that *Megf10* is expressed by brain glia[22]. To determine the subcellular localization of MEGF10 in neurons, we generated an antibody to recombinant protein (Fig. S1). MEGF10 was present both on somata of SACs and HCs and on their processes (Fig. 1f and Fig. S1). As expected, immunoreactivity levels on SACs and HCs were highest during the first postnatal week, then declined (data not shown). Thus, *Megf10* is expressed by SACs and MEGF10 protein is present on SAC processes during the time that mosaics form. Because *Megf11* expression was not observed in retina until after SAC mosaics had formed (see below), we focused first on *Megf10.*

To ask whether MEGF10 is required for SAC development, we generated mutant mice (Fig. S2). *Megf10* mutants were viable and fertile and their retinas exhibited no gross abnormalities. Mutant SACs migrated to the inner nuclear and ganglion cell layers as in controls, they were present in normal numbers, and their dendrites projected to appropriate sublaminae of the inner plexiform layer (Fig. 2a-c). Examination of whole-mounts showed, however, a dramatic loss of regular spacing among SAC somata, suggesting that their mosaic arrangement had been disrupted (Fig. 2a and Fig. S3).

To assess the degree to which SAC mosaics were disrupted, we measured the exclusion zone - the region surrounding each SAC in which other SACs are rarely found. This parameter is calculated from the density recovery profile, a plot of cell density as a function of distance from each SAC in the array[23] (Fig. 2d). The SAC exclusion zone in mutants was smaller than in wild-types, and was approximately equal to the diameter of a SAC soma (Fig. 2e).

Since the only limitation on proximity was soma size, SACs appear to be positioned randomly in *Megf10* mutants. This conclusion was supported by two additional measurements of spatial order: the packing factor[23], another index of regularity calculated from the density recovery profile; and an independent measure, the Voronoi domain regularity index, which quantifies variations in the area of the territories nearest to each cell in an array[20,24]. In each case the index calculated for SAC arrays in *Megf10* mutants was similar to that measured for computer-generated random arrays, whereas SAC arrays from wild-type littermates were highly ordered (Fig. 2f,g); heterozygotes showed a mild disorganization (Fig. S4). Together these results suggest that MEGF10 acts in SACs to impose a minimal intercellular spacing; in its absence SACs assume random positions relative to each other. By contrast, other amacrine cell types examined (Vglut3- and tyrosine hydroxylase-positive) as well as bistratified direction-selective RGCs, which are prominent synaptic targets of SACs[18], showed normal mosaic spacing (Fig 2d-g and Fig. S3).

In mice lacking the adhesion molecules Dscam or DscamL, certain retinal cell mosaics form normally, then degrade secondary to hyperfasciculation of their neurites[25,26]. To ask if MEGF10 acts in a similar indirect fashion, we labeled individual SACs in mutants. Lack of MEGF10 had no obvious effect on SAC dendritic morphology (Fig. 2h). Moreover, soma disorganization was already evident by P0 (Fig. S5), shortly after mosaics form, indicating that MEGF10 affected formation of SAC mosaics.

Next we asked whether MEGF10 is also essential for formation of the HC mosaic. Loss of MEGF10 had only a modest effect on HC regularity (Fig. 3). We therefore considered that MEGF11 might play a redundant role. *Megf11* was not expressed in embryonic retina, but it appeared in HCs and SACs during the first postnatal week and persisted into adulthood (Fig. 3a-d). Importantly, SAC mosaics begin to form before P0, but HC mosaics are established postnatally[4,6,9]. We therefore generated *Megf11* mutant mice (Fig. S2), which, like *Megf10* mutants, showed no gross retinal abnormalities (Fig. S6). Examination of HC arrays in *Megf11* mutants revealed a modest decrease in regularity similar to that in *Megf10* mutants, while in *Megf10*$^{-/-}$; *Megf11*$^{-/-}$ double mutant animals, the HC mosaic was severely disrupted (Fig. 3e-m; Fig. S7). By contrast, SACs were unaffected by loss of *Megf11* function, and were no more affected in double mutants than in *Megf10* single mutants (Figs. S6 and S8). Thus, *Megf11* is dispensable for SAC arrangement, but acts together with *Megf10* to shape the HC mosaic.

To elucidate cellular mechanisms by which *Megf10/11* act, we used a gain-of-function approach in which we introduced MEGF10 into retina by electroporation of plasmid DNA at P0. We first tested the hypothesis that MEGF10 can act as a signal that repels SACs, creating the exclusion zone that defines mosaic spacing. The electroporation method predominantly transfects dividing cells, leading to expression in neurons that exit the cell cycle postnatally such as bipolar cells, Müller glia, photoreceptors, and late-born amacrine cells[27]. Because SACs and HCs are born embryonically, they are rarely transduced[27], allowing us to surround wild-type SACs and HCs with cells ectopically expressing excess MEGF10. Indeed, electroporation of plasmid encoding a fluorescent protein (FP) or a MEGF10-FP fusion produced retinal patches in which a large fraction of neurons, but no SACs or HCs, were FP^{+} (Fig. 4a and Fig. S9). Expression of MEGF10-FP (but not FP

alone) resulted in exclusion of SACs and HCs from a swath at the edge of the electroporated patch, whereas spacing of these cells was essentially normal in patch centers (Fig. 4a,b, and Fig. S10). A truncated MEGF10 lacking the cytoplasmic domain produced an identical phenotype (Fig. S10), ruling out the possibility that MEGF10 acts indirectly by triggering production of a repellent factor by the transfected cells. Thus, MEGF10 can act as a ligand that signals to SACs and HCs.

Because MEGF10 relatives have been implicated in cell engulfment[10-13], we asked whether its overexpression formed an exclusion zone by eliminating cells. We found no evidence for cell death at patch edges (no pyknotic nuclei or activated caspase-3 immunoreactivity; data not shown). Instead, cell density was increased at the outer edge of the cell-free swath, indicating that SACs had exited the patch to create the SAC-free zone (Figs. 4b and S11). Our interpretation is that SACs and HCs are repelled by MEGF10, but within patches, the concentration of MEGF10 is similar in all directions, resulting in no net movement (Fig. 4c). Consistent with this view, SACs and HCs were entirely excluded from small patches (≤5-6 cell diameters; Fig. S10). Together these results suggest that MEGF10 can act as a repellent ligand.

We next asked which cells are sensitive to MEGF10 ligand. In *Megf10* mutants, SACs and HCs are selectively affected; this might be either because they are uniquely sensitive to MEGF10 or because only these cells encounter endogenous MEGF10 at high concentration. Ectopic expression allowed us to distinguish between these possibilities. None of 13 other amacrine, bipolar or retinal ganglion cell subtypes assayed with cell type-specific markers was detectably affected by MEGF10-FP (Fig 4d; Table S3). Thus, MEGF10 appears to act as a cell-surface ligand for a receptor specifically expressed by SACs and HCs.

Is MEGF10 the MEGF10 receptor? We used cultured epithelial cells (HEK293) to seek evidence for a MEGF10-dependent homotypic interaction. Whereas FP-expressing cells overlapped, MEGF10-FP-expressing cells formed sharp borders with narrow gaps (Fig. S12a), consistent with results in ref. 14. This “jigsaw” pattern reflected suppression or elimination of filopodia at points of intercellular apposition (Fig. S12b). Jigsaw formation and loss of filopodia required the MEGF10 cytoplasmic domain and did not occur when a MEGF10-FP-expressing cell contacted an untransfected or FP-transfected cell (Fig. S12b,c). Although we have been unable to demonstrate MEGF10 homophilic binding using biochemical methods (data not shown), these results suggest that a MEGF10-containing signaling complex mediates a homotypic interaction resulting in intercellular repulsion.

Finally, we tested the idea that MEGF10 serves as both ligand and receptor in vivo. To this end, we electroporated MEGF10 into *Megf10* mutant retina. Mutant SACs did not exit MEGF10-FP patches (Fig. 4e and Fig. S11b), indicating that *Megf10* gene function is required for SACs to respond to MEGF10 repulsive signals. Together these results suggest a model in which SACs and HCs use MEGF10 as part of a receptor complex that detects MEGF10 on their homotypic neighbors. This repulsive signal positions their somata so as to equalize MEGF10 signals on all sides, thereby creating exclusion zones (Fig. 4c).

In summary, the phenomenon of retinal mosaicism implies a molecular system for cell type-specific recognition. Several potential mechanisms have been proposed, based on imaging and computational studies, one being that short-range repulsive signals regulate tangential movements to establish each cell's territory[3,4,6-9]. To date, however, direct mediators of this phenomenon have not been described. Here we provide evidence that, for SACs and HCs, mosaic spacing requires repellent homotypic interactions mediated by MEGF10 and 11. Signals initiated by MEGF10/11 in growing neurites could lead to repositioning of the soma within the cytoplasm, perhaps by mechanisms resembling those that direct soma translocation in response to signals at the leading process of migrating neurons[28]. The finding that MEGF10 and 11 facilitate formation of three independent mosaics (two for SACs and one for HCs) appears at first to contradict the idea that mosaics are independent of each other and must therefore be regulated by distinct molecules[1,3-5]. However, because the three mosaics occupy distinct cellular planes, they may be exempt from the requirement for molecular individuation. Different molecules are likely to mediate homotypic interactions in other retinal subtypes, some of which may lead to soma translocation and others to the death of cells that violate minimal spacing[24].

Finally, we note two broader implications of our results. First, Draper/CED-1/MEGF10 homologs have so far been studied predominantly as receptors for cell engulfment[10-14]. Here we show that they also mediate cell-cell repulsion and can act as ligands as well as receptors, thereby expanding the roles for this gene family. Second, although mosaic arrangements have so far been studied formally only in retina, regularly arranged neuronal arrays are common features of central neural organization[29]. Mechanisms similar to those described here could be involved in promoting this regularity.

METHODS SUMMARY

Retinal neurons expressing fluorescent proteins were purified and used to generate aRNA for hybridizing Affymetrix microarrays as described previously[16,17]. SAC-specific genes were identified using dChip software. *Megf10* and *Megf11* mutant mice were produced from constructs generated by the Knockout Mouse Project and EUCOMM[30]. Histological methods[16,17] and methods for electroporation of plasmid DNA in vivo[17,27] were described previously. HEK293 cells (ATCC) were cultured and transfected by standard methods.

For analysis of spatial statistics, we sampled a 635.9 μm square at 3-4 locations per retina. X-Y cell coordinates, marked manually, were used to calculate Voronoi domain areas (Fiji) or DRP statistics such as the effective radius (i.e. exclusion zone) and packing factor (WinDRP). We generated random arrays matched in density and soma size to real data; these were analyzed in parallel with data from mutants. For measurement of SAC crowding in gain-of-function experiments, the Delaunay triangulation[8] was used to define each cell's nearest neighbors.

Supplementary Material

Refer to Web version on PubMed Central for supplementary material.

ACKNOWLEDGEMENTS

We thank B. Tilton, P. Rogers, J. Couget, and the Harvard GMF for technical assistance; S. Sarin and M. Yamagata for critical discussions; NIH (J.R.S.) and LSRF (J.N.K.) for funding.

Appendix

ONLINE-ONLY METHODS

Animals

CD1 and C57BL6 mice were obtained from Charles River (Wilmington, MA) and Jackson Labs. All experiments were carried out in accordance with protocols approved by the Harvard University Standing Committee on the Use of Animals in Research and Teaching.

Megf10 mutant mice were produced from a construct provided by the Knockout Mouse Project[30] (CHORI, Oakland, CA). Embryonic stem (ES) cell electroporation and chimera production were performed by the Harvard Genome Modification Facility. ES cell clones were screened for integration by PCR using primers listed in Table S4 (also see Supplementary Fig. S2). *Megf11* mutant mice were generated from gene-targeted ES cells provided by the European Conditional Mouse Mutagenesis program (EUCOMM). In both cases germline transmission was obtained from two chimeric mice generated from independent ES cell clones; each had indistinguishable phenotypes. The primers used for genotyping *Megf10* and *Megf11* mice are listed in Table S4. *Drd4-GFP* mice[31] were obtained from MMRRC.

Cell sorting and expression profiling

Retinal neurons expressing fluorescent proteins were purified as described[16,17]. Briefly, P6 retinas were dissociated, live-stained with antibodies recognizing cell surface antigens (if required for purification), and then passed through a flow cytometer (Mo Flo; Dako). Positive cells were then either: 1) plated, fixed, stained with cell-type-specific markers, and counted to assess purity; or 2) sorted directly into RNA lysis buffer (PicoPure Kit; MDS). Gene expression was profiled using Affymetrix Mouse 430 2.0 arrays, following two rounds of linear amplification (MessageAmp II; Applied Biosystems). Using these methods we generated a gene-expression database for 13 specific retinal neuron subtypes (5 amacrine, 2 bipolar, and 6 retinal ganglion cell (RGC) types; see Supplementary Table S2). SAC-specific genes (Table S1) were identified using dChip software using fold-change over other cell types as filtering criteria.

Histology and staining

Fixation and preparation of retinal cryosections was performed as described[17]. For whole-mount retinal stains, the retina was dissected out of the eyecup in a dish of phosphate buffered saline (PBS), transferred to an Eppendorf tube (up to 4 retinas per tube), and incubated at room temperature (RT) for 1 hour with agitation in blocking solution (PBS + 0.3% Triton-X100 + 3% donkey serum; Jackson Immunoresearch). Primary antibody, diluted in blocking solution, was then applied to the sample; incubation was for 6 days at 4°C with agitation. Following a 2-3 hour wash in 2-3 changes of PBS, secondary antibodies

(Jackson Immunoresearch) were applied overnight at 4°C with agitation. Following at least 4 hours of washing in PBS with agitation, retinas were flattened onto nitrocellulose membranes (Millipore) and mounted on slides (Fluoromount G; Southern Biotech). Images were acquired with a FV1000 confocal microscope (Olympus).

The following antibodies were used for immunostaining: Rabbit anti-Calbindin (Swant); goat anti-ChAT (Millipore); goat anti-VAChT (Promega); guinea pig anti-Vglut3 (Millipore); mouse anti-Islet1/2 (clone 39.4D5, Developmental Studies Hybridoma Bank; DSHB); mouse anti-Syt2 (DSHB); chicken anti-green fluorescent protein (GFP; Aves labs); rabbit anti-DsRed (Clontech); rabbit anti-beta galactosidase[32]; mouse anti-glutamine synthetase (BD); sheep anti-tyrosine hydroxylase (Millipore); mouse anti-PKC (Abcam); rabbit anti-Dab1 (Millipore); rabbit anti-Cart (Phoenix); mouse anti-Kv4.2 (Neuromabs); rabbit anti-Sox9 (Millipore); rabbit anti-cleaved caspase-3 (Cell Signaling Technology); rabbit anti-bNOS (Sigma); rabbit anti-Ebf3[17];rabbit anti-GAD65/67 (Millipore); goat anti-GlyT1 (Millipore); mouse anti-Brn3a (Millipore); mouse SMI-32 (Sternberger). MEGF10 antibody was raised in rabbits against a His-tagged peptide corresponding to amino acids 879-1130 of mouse MEGF10 (Millipore).

In situ hybridization was performed according to previously reported methods[17]. To make template for *Megf10* antisense probe, we obtained an IMAGE clone (BC075647) containing full-length mouse *Megf10* and linearized with ClaI. *Megf11* template, in pGEM-T Easy (Promega), was generated by PCR from brain cDNA using primers TGTCTTCCTTCTGCAAGCTGCTCT and ATTCCACAAGTGCCTGGTGAGTGT. Antisense riboprobes were transcribed using the DIG RNA labeling kit (Roche). Calbindin immunostaining was used to label SACs and HCs - at P0-P7 it is a selective marker for these two cell types, showing additional expression in only a small AC and RGC subset (Fig. 1, Supplementary Fig. S9, and data not shown).

Labeling of single SACs and HCs was performed by intraocular injection of low-titer adeno-associated virus, as described[33].

Quantification of mosaic regularity

For analysis of mutant phenotypes, confocal z-stacks through the GCL and INL were acquired from P14-17 retinas stained with antibodies to ChAT, Calbindin, Tyrosine hydroxylase, and/or Vglut3. Each retina was sampled in 3-4 locations (sample size was a square, 635.9 μm on each side). Stacks in which mounting artifacts introduced large local z-axis displacement of the SAC or HC array were not used. We sampled from both central and peripheral retina; despite differences in cell density between these locations the spatial organization of SAC, HC, and Vglut3 arrays did not appear to differ systematically. We therefore pooled data from central and peripheral retina for subsequent analysis. Using Fiji software, the center of each cell was marked manually to generate X-Y coordinates. The point array was flattened to a single plane without correction for local curvature, but since we only used very flat images for analysis, the spatial distortions introduced by this procedure were minor. Density recovery profiles (DRPs) were computed from these X-Y coordinates using WinDRP software[36]. Voronoi domain areas were computed in Fiji and

Microsoft Excel from the X-Y coordinate data. SAC, HC, and Vglut3$^+$ AC density and cell diameters were determined from these same images using Fiji to perform measurements.

We calculated three measures of regularity for each image. First, from the DRP, we obtained the effective radius. Effective radius gives the size of the exclusion zone - the zone in which another cell is less likely to be found than would be expected for a random array[23]. Second (also from the DRP), we computed the packing factor - a regularity index that ranges between 0 (for a random array) and 1 (for a perfect hexagonal array). Third, we calculated the Voronoi domain regularity index (VDRI) by dividing the mean Voronoi domain area for a given cellular array by the standard deviation of those areas[20,24,34].

To ascertain how the measured packing factor and VDRI compared to those that would be observed in cell arrays lacking mosaic spacing, we generated random simulations of HC, Vglut3, and SAC arrays. These simulations placed cells randomly in a 635.9μm square following a Poisson point process, until the density of the array equaled the mean density of the cell type in question. The only constraint on cell location in these simulations was soma diameter, which was calculated for each cell type as described above. The soma diameters used to constrain the simulations were 9.0μm (Vglut3 ACs), 11.0μm (SACs), and 12.2μm (HCs). Programita software[35] was used to generate the simulations (n = 10 for each cell type). Packing factor and VDRI were then calculated as described above, and the means were plotted as dashed lines in Figs 2 and 3. The VDRIs for our random simulations were similar to those calculated previously[34].

For analysis of SAC cell position in MEGF10-misexpressing retina, we acquired images at the edge of FP$^+$ or MEGF10-FP$^+$ misexpressing patches, and used the above method to obtain X-Y coordinates of all SACs in the field of view. SACs inside the patch, outside the patch, and at the edge of the patch were marked separately. “Edge” cells were defined as those outside the FP$^+$ region for which the shortest line drawn from that cell to the edge of the FP$^+$ region did not pass the soma of another SAC. To ask whether SACs were present at higher density at patch edges, we calculated the distance from each SAC to its nearest neighbors. Neighbors were defined in an unbiased manner by computing the Delaunay triangulation for the X-Y location dataset (Fiji), thereby defining line segments from each cell to its nearest neighbors.

Statistical analysis

For analysis of exclusion zone radius, packing factor, VDRI, and cell density, the significance of measured differences between genotypes was evaluated by the Mann-Whitney U test. Sample sizes were ≥ 9 images from ≥ 3 retinas per genotype (SAC and HC analysis) or 6 images from 2 retinas per genotype (Vglut3 analysis). In double-mutant experiments on HCs, the Holm-Bonferroni correction for multiple comparisons (4 different genotypes) was applied when determining significance level. For measurement of soma diameter, sample size was ≥150 cells for each genotype.

Gain-of-function experiments

A *Megf10* expression construct was generated by PCR-amplifying the open reading frame (ORF), with stop codon deleted, from the IMAGE clone described above. The open reading frame, which was predicted to encode a protein equivalent to the *Megf10* RefSeq sequence (NP_115822.1), was TA-cloned into the Gateway entry vector pCR8GW-Topo (Invitrogen). Primers used for cloning were CGATTGTTCTTCACAGAACATGGCG and TTGATGTGATTCACTGCTGCT. A cytoplasmic domain-deletion construct was made by amplifying with reverse primer TGATTCCTTCCTCTTCTGCTT to generate a truncated protein carrying only the first 9 amino acids of the intracellular domain. For expression, these constructs were transferred to a Gateway destination vector bearing the Ubiquitin-C promoter and an in-frame C-terminal GFP or monomeric Cherry tag. Mouse *Megf11* was also cloned, but pilot experiments in HEK cells suggested a lack of surface expression, so we did not attempt in vivo experiments with mouse *Megf11*.

In vivo electroporation was performed as described[17,27]. Briefly, plasmid DNA (at least 1.5 mg/mL) was injected into the subretinal space of neonatal mice (4-36 hours postpartum), and current pulses (80V) were applied across the head using paddle electrodes. We obtained identical results in MEGF10-GFP and MEGF10-Cherry misexpression experiments. Sample sizes were >20 animals each for MEGF10 misexpression and FP controls.

HEK 293 cells were cultured in DMEM with 10% fetal calf serum and transfected using TransIT reagent (Mirus). Cells were counterstained using Alexa dye-labeled cholera toxin B subunit (10μg/mL; Invitrogen), added to media 30 min prior to fixation (4% paraformaldehyde/1x PBS for 20 minutes on ice).

References in Methods section

31. Huberman AD, et al. Genetic identification of an On-Off direction-selective retinal ganglion cell subtype reveals a layer-specific subcortical map of posterior motion. Neuron. 2009; 62:327–34. [PubMed: 19447089]
32. Gray GE, Sanes JR. Lineage of radial glia in the chicken optic tectum. Development. 1992; 114:271–83. [PubMed: 1576964]
33. Hong YK, Kim I-J, Sanes JR. Stereotyped axonal arbors of retinal ganglion cell subsets in the mouse superior colliculus. J Comp Neurol. 2011; 519:1691–711. [PubMed: 21452242]
34. Whitney IE, Keeley PW, Raven M, Reese BE. Spatial patterning of cholinergic amacrine cells in the mouse retina. J Comp Neurol. 2008; 508:1–12. [PubMed: 18288692]
35. Wiegand T, Moloney A, Rings K. circles, and null-models for point pattern analysis in ecology. Oikos. 2004; 104:209–229.
36. Euler, T. WinDRP. 2003. website: http://www.mpimf-heidelberg.mpg.de/~teuler/WinDRP/ReadMe.htm

REFERENCES

1. Cook JE, Chalupa LM. Retinal mosaics: new insights into an old concept. Trends Neurosci. 2000; 23:26–34. [PubMed: 10631786]
2. Wässle H, Riemann HJ. The mosaic of nerve cells in the mammalian retina. Proc R Soc Lond B Biol Sci. 1978; 200:441–61. [PubMed: 26058]
3. Eglen SJ. Development of regular cellular spacing in the retina: theoretical models. Math Med Biol. 2006; 23:79–99. [PubMed: 16510463]

4. Reese BE, Galli-Resta L. The role of tangential dispersion in retinal mosaic formation. Prog Retin Eye Res. 2002; 21:153–68. [PubMed: 12062533]
5. Rockhill RL, Euler T, Masland RH. Spatial order within but not between types of retinal neurons. Proc Natl Acad Sci U S A. 2000; 97:2303–7. [PubMed: 10688875]
6. Huckfeldt RM, et al. Transient neurites of retinal horizontal cells exhibit columnar tiling via homotypic interactions. Nat Neurosci. 2009; 12:35–43. [PubMed: 19060895]
7. Poché R, et al. Somal positioning and dendritic growth of horizontal cells are regulated by interactions with homotypic neighbors. Eur J Neurosci. 2008; 27:1607–14. [PubMed: 18380663]
8. Galli-Resta L. Local, possibly contact-mediated signalling restricted to homotypic neurons controls the regular spacing of cells within the cholinergic arrays in the developing rodent retina. Development. 2000; 127:1509–16. [PubMed: 10704396]
9. Galli-Resta L, Resta G, Tan SS, Reese BE. Mosaics of islet-1-expressing amacrine cells assembled by short-range cellular interactions. J Neurosci. 1997; 17:7831–8. [PubMed: 9315903]
10. Wu H, -huei, et al. Glial precursors clear sensory neuron corpses during development via Jedi-1, an engulfment receptor. Nat Neurosci. 2009; 12:1534–41. [PubMed: 19915564]
11. MacDonald JM, et al. The Drosophila cell corpse engulfment receptor Draper mediates glial clearance of severed axons. Neuron. 2006; 50:869–81. [PubMed: 16772169]
12. Reddien PW, Horvitz HR. The engulfment process of programmed cell death in caenorhabditis elegans. Annu Rev Cell Dev Biol. 2004; 20:193–221. [PubMed: 15473839]
13. Hamon Y, et al. Cooperation between engulfment receptors: the case of ABCA1 and MEGF10. PLoS One. 2006; 1:e120. [PubMed: 17205124]
14. Suzuki E, Nakayama M. MEGF10 is a mammalian ortholog of CED-1 that interacts with clathrin assembly protein complex 2 medium chain and induces large vacuole formation. Exp Cell Res. 2007; 313:3729–42. [PubMed: 17643423]
15. Sanes JR, Zipursky SL. Design principles of insect and vertebrate visual systems. Neuron. 2010; 66:15–36. [PubMed: 20399726]
16. Kay JN, et al. Retinal ganglion cells with distinct directional preferences differ in molecular identity, structure, and central projections. J Neurosci. 2011; 31:7753–62. [PubMed: 21613488]
17. Kay JN, Voinescu PE, Chu MW, Sanes JR. Neurod6 expression defines new retinal amacrine cell subtypes and regulates their fate. Nat Neurosci. 2011; 14:965–972. [PubMed: 21743471]
18. Demb JB. Cellular mechanisms for direction selectivity in the retina. Neuron. 2007; 55:179–86. [PubMed: 17640521]
19. Haverkamp S, Wässle H. Immunocytochemical analysis of the mouse retina. J Comp Neurol. 2000; 424:1–23. [PubMed: 10888735]
20. Keeley PW, Whitney IE, Raven MA, Reese BE. Dendritic spread and functional coverage of starburst amacrine cells. J Comp Neurol. 2007; 505:539–46. [PubMed: 17924572]
21. Elshatory Y, et al. Islet-1 controls the differentiation of retinal bipolar and cholinergic amacrine cells. J Neurosci. 2007; 27:12707–20. [PubMed: 18003851]
22. Cahoy JD, et al. A transcriptome database for astrocytes, neurons, and oligodendrocytes: a new resource for understanding brain development and function. J Neurosci. 2008; 28:264–78. [PubMed: 18171944]
23. Rodieck RW. The density recovery profile: a method for the analysis of points in the plane applicable to retinal studies. Vis Neurosci. 1991; 6:95–111. [PubMed: 2049333]
24. Raven MA, Eglen SJ, Ohab JJ, Reese BE. Determinants of the exclusion zone in dopaminergic amacrine cell mosaics. J Comp Neurol. 2003; 461:123–36. [PubMed: 12722109]
25. Fuerst PG, Koizumi A, Masland RH, Burgess RW. Neurite arborization and mosaic spacing in the mouse retina require DSCAM. Nature. 2008; 451:470–4. [PubMed: 18216855]
26. Fuerst PG, et al. DSCAM and DSCAML1 function in self-avoidance in multiple cell types in the developing mouse retina. Neuron. 2009; 64:484–97. [PubMed: 19945391]
27. Matsuda T, Cepko CL. Electroporation and RNA interference in the rodent retina in vivo and in vitro. Proc Natl Acad Sci U S A. 2004; 101:16–22. [PubMed: 14603031]
28. Solecki DJ, Model L, Gaetz J, Kapoor TM, Hatten ME. Par6alpha signaling controls glial-guided neuronal migration. Nat Neurosci. 2004; 7:1195–203. [PubMed: 15475953]

29. Budry L, et al. Related pituitary cell lineages develop into interdigitated 3D cell networks. Proc Natl Acad Sci U S A. 2011; 108:12515–20. [PubMed: 21746936]

30. Skarnes WC, et al. A conditional knockout resource for the genome-wide study of mouse gene function. Nature. 2011; 474:337–42. [PubMed: 21677750]

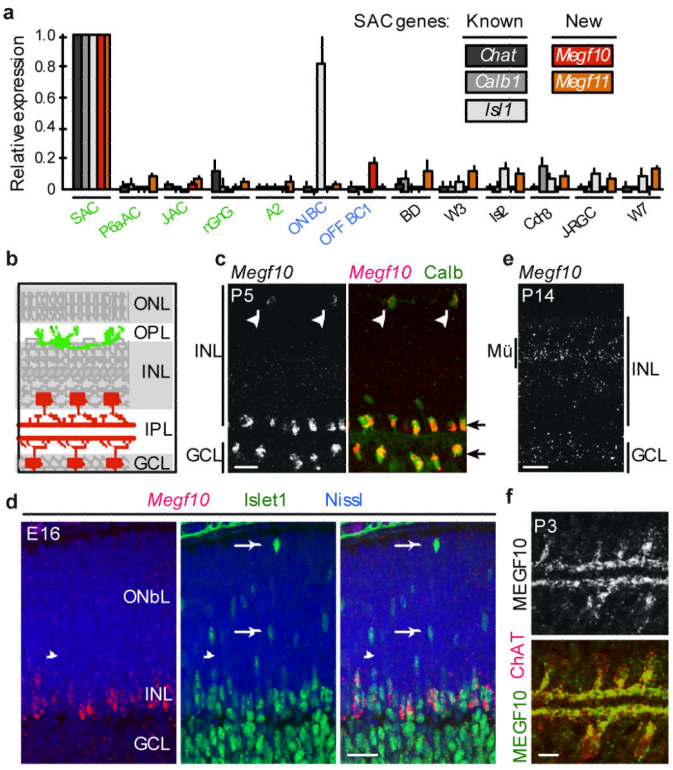

Figure 1.

Expression of *Megf10* and *Megf11* in SACs and HCs.

a. Relative expression level of *Megf10*, *Megf11*, and the known SAC markers *Chat*, *Calb1* (encoding Calbindin), and *Isl1* (Islet1) in thirteen amacrine (green), bipolar (blue) and retinal ganglion cell (black) subtypes analyzed with microarrays. Level in SACs set to 1 for each gene. *Isl1* was also detected in ON bipolar cells as previously reported[21]. Abbreviations for subtypes are defined in Supplementary Table S2.

b. Schematic of retina. ONL, outer nuclear layer containing photoreceptors; OPL, outer plexiform layer with photoreceptor synapses; INL, inner nuclear layer with horizontal, bipolar, amacrine, and Müller glial cells; IPL, inner plexiform layer with synapses among bipolar, amacrine and ganglion cells; GCL, ganglion cell layer including displaced amacrine cells. SACs (red), HCs (green), and Müller cells (dark gray row) are indicated.

c. In situ hybridization for *Megf10* (left panel; red in right panel) combined with anti-Calbindin immunohistochemistry (green in right panel) at P5 shows expression in SACs (black arrows) and HCs (arrowheads).

d. *Megf10* (red) in E16 retina. Islet1 (green) marks SACs migrating through the outer neuroblast layer (ONbL) and in the INL[9]. *Megf10* (red) is expressed by migrating SACs as they arrive in the INL (arrowhead), but not at earlier stages of their migration through the ONbL (arrows).

e. *Megf10* expression appears in Müller glia (Mü) and is lost from SACs and HCs by P14.

f. Double-label immunostaining for MEGF10 (green) and ChAT (red). MEGF10 protein localizes to somata and processes of developing SACs (also see Fig. S1).

Scale bars, 20 μm (**c-e**) or 10 μm (**f**).

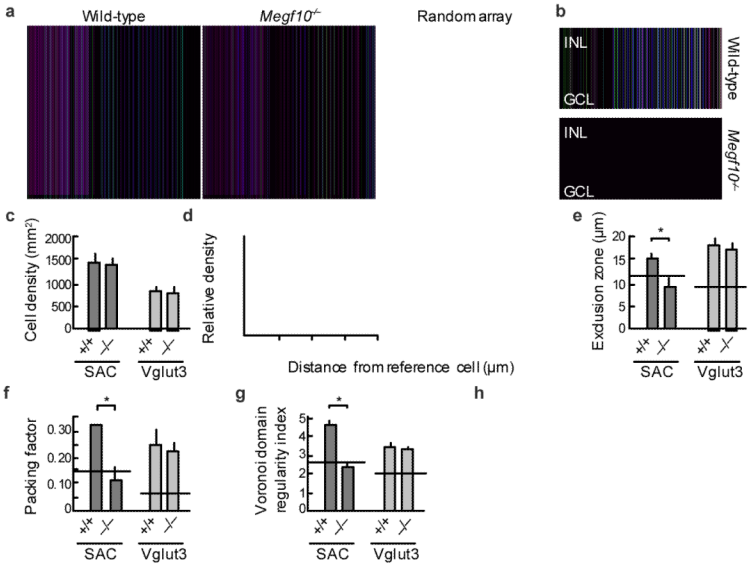

Figure 2.

Loss of SAC mosaic spacing in *Megf10* mutant mice

a. SAC mosaic in inner nuclear layer (INL) of wild-type (left) and *Megf10*$^{-/-}$ (center) retina, revealed by whole-mount staining with anti-ChAT. Wild-type mice have evenly spaced SAC somata, whereas mutants exhibit clumps and gaps similar to those seen in a simulation of a random cellular array (right). See Figure S3 for similar results in ganglion cell layer (GCL) SACs.

b. ChAT-stained retinal sections from wild-type and *Megf10* mutant animals. Laminar positions of SAC somata and processes are normal in mutants, even in regions where somata are clumped.

c. Density of SACs and Vglut3^{+} amacrines is similar in wild-type (+/+) and *Megf10* mutant (-/-) retina.

d. Density recovery profiles (DRPs) for the SAC (INL) and Vglut3^{+} amacrine arrays. Graphs show the density of cells in a ring of radius *x*, relative to the density of cells in the image as a whole. Dashed line, DRP of random point array. The exclusion zone characteristic of mosaic spacing is measured as a dip below this line.

e: Exclusion zone radius measured from (**d**). Dashed line, expected result for an array of cells distributed randomly, i.e. the diameter of a single cell. Increases above this minimum indicate spatial order. The mutant SAC exclusion zone radius was similar in size to a SAC cell diameter, and was significantly smaller than wild-type (*$p < 0.0001$). Vglut3^{+} amacrine exclusion zones were unaffected.

f, g. SAC packing factor (**f**) and Voronoi domain regularity index (**g**) were significantly lower in *Megf10*$^{-/-}$ mice than in wild-type littermates (*$p < 0.0001$). Dashed line, mean for arrays of cells distributed randomly. Wild-type SACs, and Vglut3^{+} cells of both genotypes, were non-randomly arrayed. The SAC array in mutants was not significantly different from random arrays (**f**, $p = 0.16$; **g**, $p = 0.48$).

h. Morphology of single GCL SACs, labeled with adeno-associated virus driving membrane-targeted Cherry fluorescent protein, showed no gross abnormalities in *Megf10* mutants ($n \geq 8$ cells each genotype).

Data from P15 (**a-g**) or P80 (**h**) mice. Scale bars, 50 μm. Error bars, s.e.m.

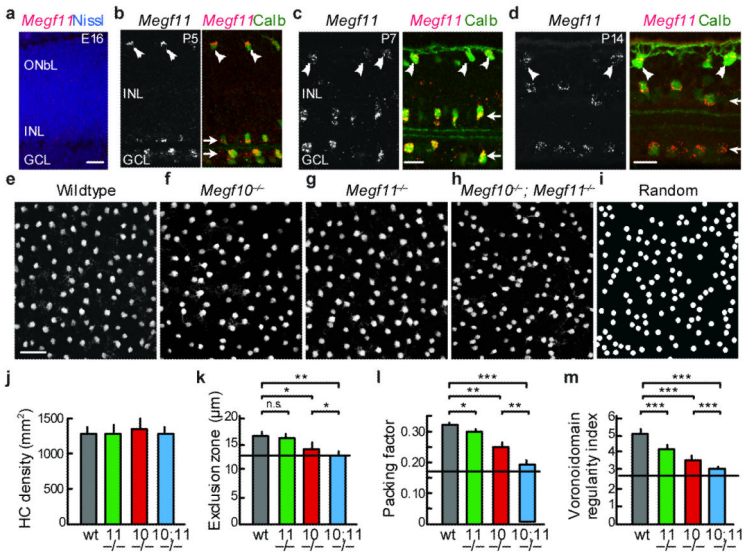

Figure 3.

Horizontal cell mosaic spacing requires *Megf10* and *Megf11*.

a-d. In situ hybridization for *Megf11* at ages indicated. *Megf11* (red) was not expressed at E16 (**a**). Calbindin immunostaining (green) labels SACs and HCs, which co-express *Megf11* at P5 (**b**), P7 (**c**), and P14 (**d**). See Fig. 1 for abbreviations.

e-i. Retinal whole-mounts stained for Calbindin to reveal the HC array. In wild-type mice (**e**), HCs are distributed evenly. *Megf10*$^{-/-}$ mutants (**f**) and *Megf11*$^{-/-}$ mutants (**g**) show subtle changes in the regular spacing of HCs, while double *Megf10*$^{-/-}$; *Megf11*$^{-/-}$ mutants (**h**) show striking HC disorganization similar to a simulation of a random HC array (**i**).

j-m. Quantification of HC spacing regularity in *Megf10*$^{-/-}$ (red) or *Megf11*$^{-/-}$ (green) single mutants; *Megf10*$^{-/-}$; *Megf11*$^{-/-}$ double mutants (blue); and wild-type siblings (gray). In all genotypes, HCs were present at normal density (**j**) but were less regularly spaced relative to wild-type based on exclusion zone radius (**k**), packing factor (**l**), and Voronoi domain regularity (**m**) measurements as in Fig. 2. Double mutants showed significantly less order than single *Megf10*$^{-/-}$ or *Megf11*$^{-/-}$ mutants and approach random arrangement indicated by dashed lines (**k**, mean HC soma diameter; **l,m**, computed values for random arrays. P-values: *p < 0.01, **p <0.001, ***p< 0.0001. n.s. = not significant. Error bars give s.e.m. Data in **e-m** from P15 animals. Scale bars, 20 µm (**a-d**; **b**,**c** share scale) or 50 µm (**e-i**).

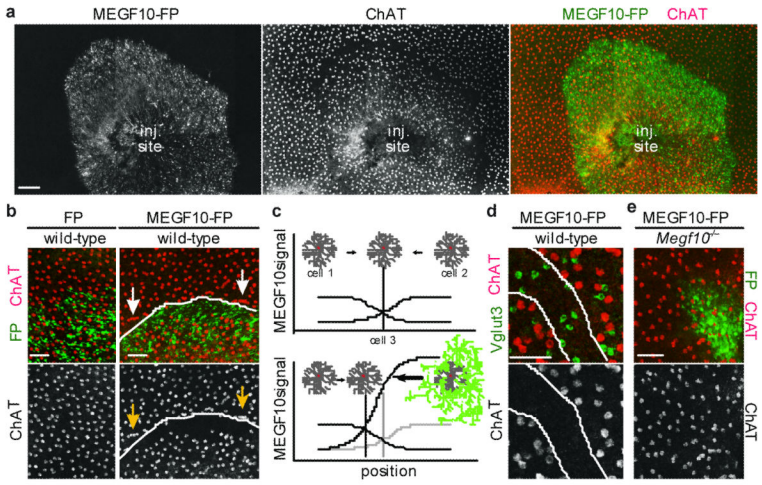

Figure 4.

MEGF10 acts as both ligand and receptor to trigger SAC repulsion.

a: A retinal patch transfected by electroporation with plasmid encoding MEGF10-FP fusion protein, viewed in flatmount. SAC somata in INL, stained with anti-ChAT, are excluded from a swath at the patch edge. SACs are evenly spaced elsewhere, except where the retina was pierced to inject DNA (inj. site).

b: Higher-magnification views of patch edges. FP misexpression (left) did not affect SAC spacing, but MEGF10-FP (right) produced a SAC-free zone just inside the transfected region and induced apparent crowding of SACs immediately outside it (arrows). Dashed line, patch edge. See Fig. S11 for quantification of cell distribution at patch edges.

c. Hypothesis for MEGF10 function based on **a,b**. In wild-type retina (top), SACs use MEGF10 as a ligand to signal their location to neighboring SACs. Cell 3 positions itself at the point where repulsive signals on either side (from Cell 1 and Cell 2) are equal. In MEGF10-FP overexpression (bottom), that location is now outside the patch.

d. MEGF10-FP transfected whole-mount immunostained for ChAT and Vglut3. Dashed lines mark SAC-free zone (see Fig. S10). Vglut3^{+} ACs are present in this zone.

e. MEGF10-FP is incapable of generating a SAC-free zone when misexpressed in *Megf10* mutant retina, indicating that MEGF10 is needed for SAC responses to MEGF10. See Fig. S11 for quantification.

Scale bars, 100 μm (**a**); 50 μm (**b,d**). All retinas from P10-P15 animals.